Design Studies of Low-Aspect Ratio Quasi-Omnigenous Stellarators

D. A SPONG, S. P. HIRSHMAN, J. C. WHITSON, D. B. BATCHELOR, RECEIVED
B. A. CARRERAS, V. E. LYNCH, J. F. LYON, P. M. VALANJU,[1] W. MINER,[2] P. MOROZ,[2]
M. C. ZARNSTORFF,[3] D. A. MONTICELLO,[3] A. S. WARE,[4] L. GARCIA[5]   NOV 2 4 1998

Oak Ridge National Laboratory   OSTI
P. O. Box 2009
Oak Ridge, Tennessee 37831-8071

Abstract

Significant progress has been made in the development of new modest-size compact stellarator devices that could test optimization principles for the design of a more attractive reactor. These are 3 and 4 field period low-aspect-ratio quasi-omnigenous (QO) stellarators based on an optimization method that targets improved confinement, stability, ease of coil design, low-aspect-ratio, and low bootstrap current.

1. CONFIGURATION OPTIMIZATION

Development of increasingly sophisticated optimization methods in recent years [1,2,3] allows the design of stellarators that could lead to an attractive fusion power plant. Improved plasma confinement is achieved either through targeting symmetries (e.g., either helical [4] or toroidal [5]) of |B| in Boozer magnetic coordinates [6] or by directly attempting to reduce the deviation of particle guiding-center orbits away from flux surfaces [7]. Our stellarator optimization technique follows the latter approach through targeting the alignment of second adiabatic invariant J* [8] contours for the trapped particle population with magnetic flux surfaces (known as QO or quasi-omnigeneity). As this optimization method has evolved, additional physics and engineering targets have been included, such as Mercier stability, rotational transform $\iota(r) = 1/q$ in the range of 0.5 to 0.8 with $< 30\%$ from plasma current, good coil realizability, low ripple, and ballooning and kink stability.
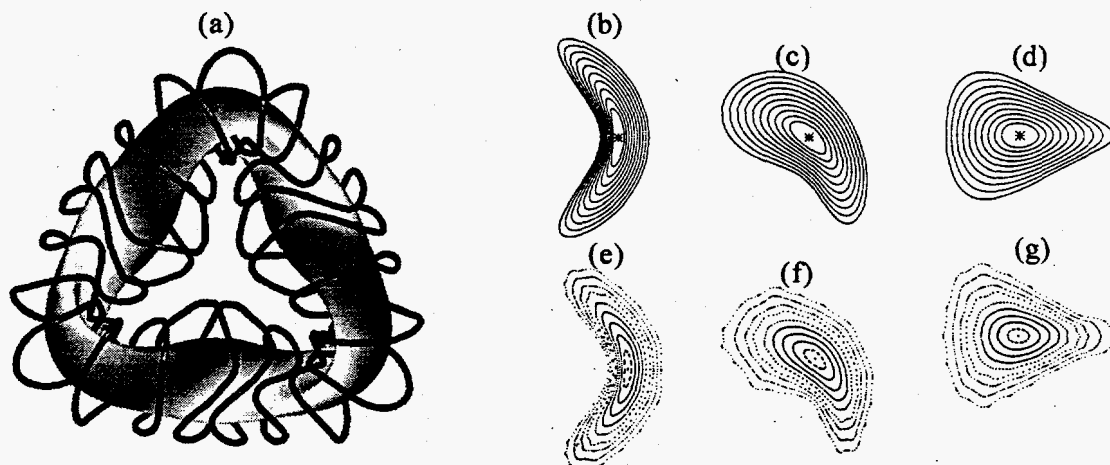

FIG. 1 (a) – Outer flux surface and modular coils for an $N_{fp} = 3$ QO device, (b), (c), (d) - VMEC flux surfaces for this configuration at toroidal angles $\zeta/N_{fp} = 0°$, $90°$, and $180°$, (e), (f), (g) -Flux surfaces reconstructed from following field lines based on the modular coil configuration at $\zeta/N_{fp} = 0°$, $90°$, and $180°$.

---

[1] University of Texas, Austin, Texas
[2] University of Wisconsin, Madison, Wisconsin
[3] Princeton Plasma Physics Laboratory, Princeton, New Jersey
[4] University of Montana, Missoula, Montana
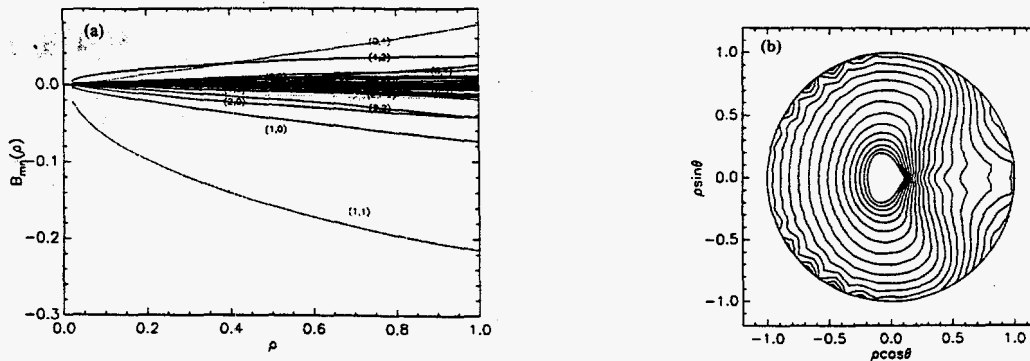[5] Universidad Carlos III de Madrid, Madrid, Spain.

FIG. 2 (a) - B_{mn} profiles for an $N_{fp} = 3$, $R_0/a = 3.6$ device, (b) - J* contours for trapped particles $(\varepsilon/\mu \approx 1.0 \, T)$ for the same device.

Our optimization is comprised of: (a) an adjustment of the outer magnetic surface shape and plasma current profile to achieve the desired physics goals, followed by (b) a synthesis of the modular magnetic coil geometry which produces that outer surface shape. Our earlier studies [1,2] produced low-aspect-ratio stellarator configurations that had promising features for a reactor (stable at $<\beta> \, >7\%$, low bootstrap current, and reasonable confinement), but they were not self-consistent or optimized for an experimental test at modest scale. With development of a modest experiment in mind, our recent QO optimizations have focused on $N_{fp} = 3$, 4 devices (N_{fp} = field periods) because they seem to provide a good compromise between the achievement of desired physics properties and simple coil configurations with adequate plasma/coil spacing. In this paper we analyze both $N_{fp} = 3$ ($R_0/a = 3.6$) and $N_{fp} = 4$ ($R_0/a = 4.2$) devices for the parameters of $R_0 = 1$ m, $B_0 = 1$ T. The ι profile for $N_{fp} = 3$ varies from 0.55 to 0.64 while that for $N_{fp} = 4$ varies from 0.68 to 0.78. The flux surfaces for the $N_{fp} = 3$ device are shown in Fig. 1 while the B_{mn} spectrum is shown in Fig. 2(a). The helical m = 1, n = 1 component is dominant, but not to the same degree as in a quasi-helical device. There is a residual mirror field (m = 0, n = 1), which is the dominant component in W7-X [3]. The present configurations arose from a large R_0/a (>5), nearly quasi-helical state, by reducing R_0/a while trying to retain J* = J*(ψ). Trapped particle orbits approximately follow the J* contours [Fig. 2(b)] in their bounce precessional motion; our optimization attempts to make the J* contours over a range of ε/μ values as nearly circular and closed as possible.

2. NEOCLASSICAL TRANSPORT

The QO optimization technique is expected to lead directly to reductions in neoclassical transport because cross-field drifts scale with $<v_p \bullet \nabla \psi> \propto \partial J^*/\partial \theta$. While empirical transport scalings such as ISS95 [9] may be expected for a QO experiment, it is desirable to minimize neoclassical transport well below this level in order that any enhanced confinement regimes will lead to a measurable improvement. In Fig. 3(a) we plot the density dependence of the Monte Carlo particle diffusion coefficient for $N_{fp} = 3$ and 4 devices. These have been calculated using 2000 particles at zero ambipolar electric field and a constant plasma temperature of 1 keV (the test particles are monoenergetic at 2 keV). The diffusivities show a drop-off with decreasing collisionality without evidence of a ripple-induced (i.e., $1/\nu$) scaling. By calculating a sequence of such monoenergetic diffusivities over a range of energies we integrate to obtain the transport coefficients for a Maxwellian distribution. This has been carried out for the $N_{fp} = 4$ device at a density of 5×10^{13} cm^{-3} and as a function of the ambipolar electric field. Using this sequence, we obtain the heat conductivity by taking the energy moment [Fig. 3(b)]. The 0-D energy confinement time $\tau_E \approx a^2/4\kappa$ is plotted based on this heat conductivity. For comparison, the empirical ISS95 lifetime $\tau_{E,ISS95} = 11.4$ msec for these parameters (B = 1T, $<a> = 0.23$m, n = 5×10^{13}cm^{-3}) roughly equals the neoclassical confinement time in the absence of an electric field. Ambipolar electric fields in the range $e\phi/kT_{ion}(r = a) \approx 2$ to 3 are expected where, from Fig.3(b), $\tau_{E,neo} = (2-3)\tau_{E,ISS95}$.

DISCLAIMER

DISCLAIMER

Portions of this document may be illegible in electronic image products. Images are produced from the best available original document.
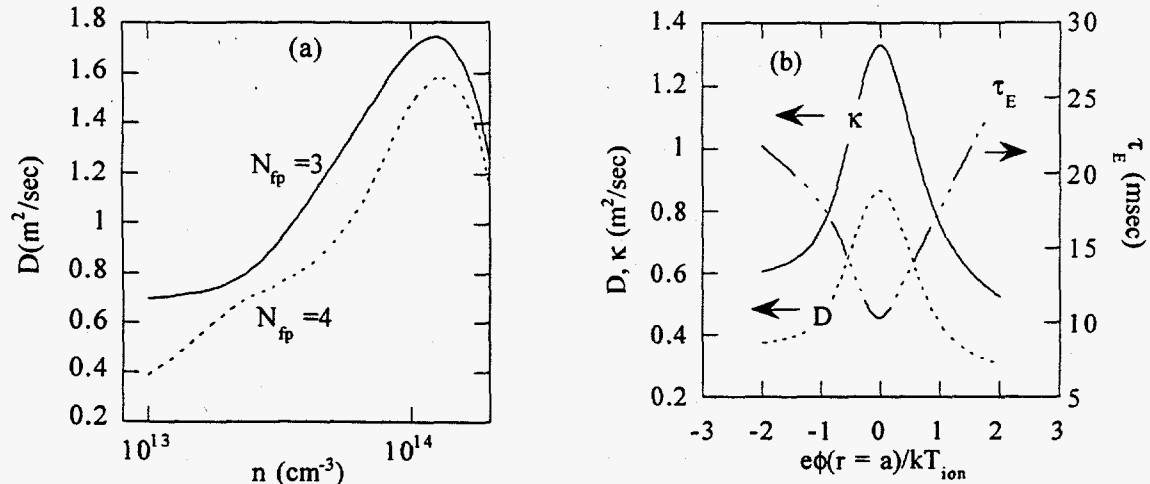
FIG. 3 (a) - Density scaling of neoclassical diffusion coefficient based on monoenergetic Monte Carlo calculation, (b) - Electric field scaling of neoclassical diffusion, heat conductivity and 0-D energy lifetimes (τ_E) for a Maxwellian distribution.

3. ENERGETIC PARTICLE CONFINEMENT AND HEATING

The ability to heat toroidal plasmas depends critically on the confinement of energetic tail populations, which is a major motivation for our confinement optimization. We have particularly focused on the confinement of trapped energetic ions such as would be produced by ICRF heating. We have examined the confinement of this population by following an ensemble of collisionless particles and recording their loss rates vs. time. All particles are launched at a specified energy at resonant locations where $B = B_{resonant}$ with $\varepsilon/\mu = B_{resonant}$ [i.e., the particles have their turning points ($v_\parallel = 0$) at the resonant field]. Orbit losses occur both from open J* contours and from deviations of the guiding center orbits away from the J* surfaces. These orbit deviations are proportional to the particle's drift per bounce which scales as ρ/a, the ratio of the gyroradius to the minor radius. In Fig. 4(a) we show results from following about 500 collisionless ions at 20 keV for flux surfaces in the inner 50% of the minor radius in our $N_{fp} = 4$ configuration. We vary the resonant field $B_{resonant}$ from 0.9 T up to 1.15 T. This selects different starting locations for the ions as well as different values of ε/μ (and thus different J* contours). Confinement depends sensitively on the value of $B_{resonant}$. This dependence arises from the variation of the J* contours as ε/μ is changed.
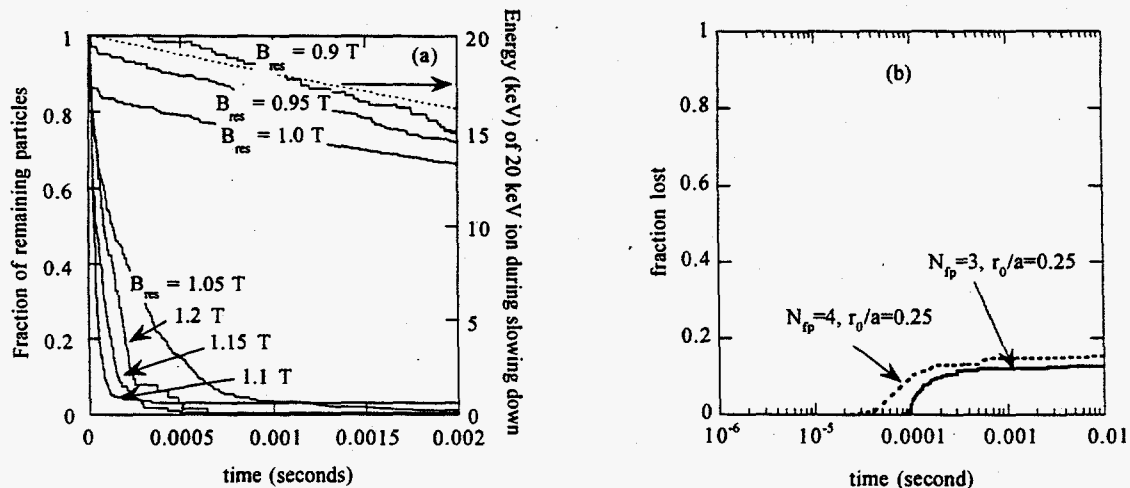

FIG 4 (a) - Fraction of 20-keV ICRF resonant ions confined vs. time for an $N_{fp} = 4$ device ($B_0 = 1$ T), for different values of $\varepsilon/\mu = B_{res}$, (b) - Fraction of 3.5-Mev α-particles lost vs. time for reactor scale versions of the $N_{fp} = 3$ and 4 devices, starting particles at r/a = 0.25.

For $\varepsilon/\mu < 1$ T the J* contours are relatively well closed, whereas for 1.05 T $< \varepsilon/\mu < 1.15$ T there begin to be open contours which cause prompt particle losses. The dashed line in Fig. 4(a) indicates the rate at which a 20 keV ion collisionally slows down in a $T_e = 1$ keV background plasma; for the better confined cases, the particle loss approximately parallels the slowing-down rate, implying effective ICRF heating at these resonances. The other parameter which influences ion confinement is ρ/a; this determines the degree to which the particle orbit deviates from constant J* contours. Increasing the magnetic field from 1 to 2 T uniformly improves energetic particle confinement for both $N_{fp} = 3$ and 4 devices. We have applied this calculation to the CHS configuration ($N_{fp} = 8$) in which ICRF heating was successfully used. We find that the confinement in our configurations generally exceeds that calculated for CHS, leading us to conclude that trapped ion confinement should be adequate for ICRF heating.

We have also scaled these configurations to reactor sizes ($B_0 = 5$ T, $R_0 = 10$ m) to check α-particle confinement [Fig. 4(b)]. These calculations are based on following a group of about 500 collisionless α-particles ($E_0 = 3.5$ MeV) born at $r/a = 0.25$. The impact of these levels of α-particle losses is not expected to be a major issue for the power balance, but will need further analysis with respect to localization of power loading on the first wall.

4. STABILITY

Our optimization procedure checks for the existence of a magnetic well, in addition to favorable Mercier and ballooning stability over the whole plasma radius. Ballooning β thresholds for the $N_{fp} = 3$ and 4 configurations discussed above are approximately 2% and 2.5%, respectively, which is adequate for a test in a modest experiment. Typically, for broad pressure profiles, a region near the edge goes unstable first. Several methods have been successfully used in our previous configurations to extend the stable window into the $<\beta> = 5$ to 6% range, including profile flattening, increased shear in the ι profile, and boundary shaping. A fast hybrid finite difference/variational version of the ballooning calculation has recently been developed which should facilitate improved optimization of the ballooning stability limit. In addition, low-n pressure-driven instabilities have been analyzed with a 3D initial value MHD model [10]. The low-n radial mode structure shows similar structure as the radial dependence of the high-n ballooning growth rate.

5. CONCLUSIONS

We have studied a range of attractive low field period ($N_{fp} = 3 - 4$) devices for testing the QO optimization technique. Our method targets improvements in energetic particle confinement, core transport, stability, ease of coil design, and low aspect ratio. Modular coil sets exist which produce our optimized systems and these both preserve the original flux surfaces as well as the optimized physics properties. This optimization effort is ongoing and we expect to further address such issues as ballooning stability optimization, self-consistent bootstrap current equilibria, and a more comprehensive modeling of transport and ICRF heating.

[1] HIRSHMAN, S. P., et al, Phys. Rev. Lett. **80** (1998) 528.
[2] SPONG, D. A., et al, Physics of Plasmas **5** (1998) 1752.
[3] GORI, S., et al, Theory of Fusion Plasmas (Varenna, 1996), Editrice Compositori, Bologna (1997) 335.
[4] NÜHRENBERG, J., ZILLE, R., Phys. Lett. **A129** (1988) 113.
[5] GARABEDIAN, P. R., Phys. Plasmas **3** (1996) 2483.
[6] BOOZER, A .H., Phys. Fluids **23**, (1980) 904.
[7] CARY, J. R., et al, Phys. Rev. Lett. **78** (1997) 674; also see: SKOVORODA, A. A., et al, Plasma Physics Reports **21** (1995) 937; and WEITZNER, H., Phys. of Plasmas, **4** (1997) 575.
[8] ROME, J. A., Nuclear Fusion **35** (1995) 195; also, Cary, J. R., et al, J. Phys. Fluids **31** (1988) 1586.
[9] STROTH, U., et al, Nuclear Fusion **36** (1996) 1063.
[10] GARCIA, L., SANCHEZ, R., JIMENEZ, J. A., J. Plasma Fus. Res. Series **1** (1998) 468.